ADVANCED OPTICAL MATERIALS
www.advopticalmat.de

Multifunctional Metasurface Design with a Generative Adversarial Network

Sensong An, Bowen Zheng, Hong Tang, Mikhail Y. Shalaginov, Li Zhou, Hang Li, Myungkoo Kang, Kathleen A. Richardson, Tian Gu, Juejun Hu, Clayton Fowler, and Hualiang Zhang**

Metasurfaces have enabled precise electromagnetic (EM) wave manipulation with strong potential to obtain unprecedented functionalities and multifunctional behavior in flat optical devices. These advantages in precision and functionality come at the cost of tremendous difficulty in finding individual meta-atom structures based on specific requirements (commonly formulated in terms of EM responses), which makes the design of multifunctional metasurfaces a key challenge in this field. In this paper, a generative adversarial network that can tackle this problem and generate meta-atom/metasurface designs to meet multifunctional design goals is presented. Unlike conventional trial-and-error or iterative optimization design methods, this new methodology produces on-demand free-form structures involving only a single design iteration. More importantly, the network structure and the robust training process are independent of the complexity of design objectives, making this approach ideal for multifunctional device design. Additionally, the ability of the network to generate distinct classes of structures with similar EM responses but different physical features can provide added latitude to accommodate other considerations such as fabrication constraints and tolerances. The network's ability to produce a variety of multifunctional metasurface designs is demonstrated by presenting a bifocal metalens, a polarization-multiplexed beam deflector, a polarization-multiplexed metalens, and a polarization-independent metalens.

Metasurfaces, the 2D versions of metamaterials, are planar/conformal devices composed of subwavelength structures, called meta-atoms,[1,2] which are capable of tailoring amplitude, phase, polarization, and angular momentum of incident waves.[3–6] By manipulating the geometry of the individual meta-atom, independent phase and amplitude control of electromagnetic (EM) field can be achieved. Recently, metasurfaces consisting of all-dielectric meta-atoms have drawn enormous attention,[4,7,8] due to their unique capability of supporting EM multipole resonances and significantly lower losses as compared to their metallic counterparts.[9–12] The multipole responses in a meta-atom can be highly complicated, even for simple shapes, and thus an arbitrary meta-atom's response to an incident EM wave is difficult to predict. Traditional design approach relies on empirical reasoning or trial-and-error,[4,8] which is inefficient and often ineffective, since this approach involves tremendous numerical full-wave simulations (e.g., finite-element method, finite-difference time-domain method, and finite integration technique), which provide accurate predictions but are extremely time consuming. Therefore, it can be time-consuming and laborious to find an appropriate set of meta-atoms for a specific design. Meanwhile, multifunctional metasurfaces such as multi-wavelength metasurfaces,[9,10,13,14] multi-polarization metasurfaces,[15] or reconfigurable metasurfaces based on phase change materials,[16–21] have presented another major design challenge due to the difficulty in exploring vast parameter spaces containing meta-atoms that possess sufficient complexity to satisfy restrictive design requirements. Therefore, in addition to exploring meta-atoms with basic shapes such as rings,[9,10] cubes,[14,22] or cylinders,[23] previous works have also adopted evolutionary algorithms to search for meta-atoms and metasurface with free-form patterns[13,15,24–27] which provides additional degrees of freedom (DOF). Nevertheless, the capability of this approach largely depends on the quality of the initial guess, which limited their stability and efficacy as the complexity of the problem grows.

To address the challenges in designing non-intuitive meta-atom and metasurfaces, several deep neural network based approaches have been proposed and investigated since 2018. A "tandem" network structure[28–39] combining a pre-trained

S. An, B. Zheng, H. Tang, L. Zhou, H. Li, Dr. C. Fowler, Prof. H. Zhang
Department of Electrical and Computer Engineering
University of Massachusetts Lowell
Lowell, MA 01854, USA
E-mail: clayton_fowler@uml.edu; hualiang_zhang@uml.edu
Dr. M. Y. Shalaginov, Dr. T. Gu, Prof. J. Hu
Department of Materials Science and Engineering
Massachusetts Institute of Technology
Cambridge, MA 02319, USA
Dr. M. Kang, Prof. K. A. Richardson
CREOL
University of Central Florida
Orlando, FL 32816, USA
The ORCID identification number(s) for the author(s) of this article can be found under https://doi.org/10.1002/adom.202001433.

DOI: 10.1002/adom.202001433

simulator with another model generator overcomes the issue of non-unique solutions (common to all inverse design problems), and allows the inverse neural network to converge steadily. However, there are several limitations to this approach. First, the designs constructed via tandem networks are dealing with variations of simple canonical geometries defined by a few parameters. The examples of such geometries include planar layers,[28] metallic bars,[31] dielectric spheres,[32] and cylinders.[33] The lack of available DOF restricts functionality and performance of the designed metasurface. Training of the tandem networks can be extremely difficult, if not impossible, for meta-atoms with free-form geometries because of the dimension mismatch between the small number of EM response inputs (1D spectrum) and large design parameter outputs (2D images). Therefore, such tandem inverse design networks can only generate a single design based on each input setting, which suggests that the networks are "memorizing" the results rather than "learning" the design mechanisms and "composing" new solutions.

Generative adversarial network (GAN) provides a promising solution to mitigate these limitations. Since GANs were first introduced in 2014,[40] they have been widely applied in the field of image processing, due to their unique ability to reveal the hidden distributions behind enormous training datasets and compose complex and diverse designs based on limited inputs. Through Conditional Generative Adversarial Nets (CGAN)[41] (a GAN variant that is able to generate required designs conditioned on class labels), several design networks have been developed for realizing metallic metasurface filters with defined transmissive,[29] reflective[29,42,43] or emissive[44] spectra and dielectric meta-gratings with specified beam deflection angles and working frequencies.[45–47] However, these existing GAN-enabled metasurface design networks deal with either only amplitude responses[29,42,43,48–52] or with reduced dimensionality structures (1D meta-grating designs at a supercell level[26,45,46]). Due to the hardly-predictable phase jumps caused by EM poles,[33] a GAN-enabled meta-atom design approach that deals with both amplitude and phase responses has been challenging and critical (since most optical metasurfaces reshape the wavefront of the incident light by introducing local variations in both phase and amplitude). The GAN-enabled design of multifunctional metasurfaces has become even more challenging and until this work, has remained an open question.

In this work, we present a novel approach for designing free-form all-dielectric metasurface devices by combining the CGAN with the Wasserstein Generative Adversarial Networks (WGAN).[53,54] As another widely-adopted GAN variant, WGAN introduces earth-mover distance as a loss evaluation method, which not only stabilizes the training process, but also qualifies the network for handling comprehensive metasurface design problems. Moreover, the proposed approach handles multiple inputs in parallel, meaning that the complexity is not affected by the size of the inputs. This feature further positions this GAN-based approach as the preferred solution in tackling multifunctional inverse design problems. Based on this highly efficient network, we have designed and verified several multifunctional metasurfaces, including a bifocal lens, a polarization-multiplexed beam deflector and two multifunctional metalenses in order to illustrate the versatility and scalability of the proposed method (some of these results are included in the Supporting Information). The presented examples substantiate that our approach demonstrates several important milestones as 1) the first free-form all-dielectric meta-atom design network; 2) the first free-form multifunctional metasurface design network and 3) the first metasurface lens designed by GANs.

The proposed network (**Figure 1**) combines the WGAN structure with the method of a CGAN, which trains a generator that maps a set of design conditions, x, combined with a Gaussian noise vector, z, to produce a target design (or fake samples), y', defined as: $y' = G(z|x)$. We treated each meta-atom as a 2D image and all meta-atoms are of the same height. In general, the conditions x can be any kind of auxiliary information. In this case, x carries the EM responses obtained from numerical simulations of real samples y. The discriminator calculates the Wasserstein distance between the real samples y and the generated fake ones y', then it inversely tunes the parameters within the generator/discriminator network to minimize/maximize the Wasserstein distance by using a gradient descent algorithm. The Wasserstein distance between a target design $y \in P_{\text{data}}$, and a generated one $y' \in P_{\text{G}}$, is defined as:

$$W(P_{\text{data}}, P_{\text{G}}) \approx \sup_{\|D\|_{\text{L}} \leq 1} \left\{ \mathbb{E}_{y \sim P_{\text{data}}} \left[D(y|x) \right] - \mathbb{E}_{y' \sim P_{\text{G}}} \left[D(y'|x) \right] \right\} \tag{1}$$

where P_{data} and P_{G} are the sets of EM responses extracted from the training data and produced by the generator, respectively; E stands for the expected value and D is the Wasserstein distance given by the discriminator.

The parameter optimizations for the generator and the discriminator are processed in turns, aiming for opposite objectives: The generator G is trained to produce samples that cannot be distinguished by the discriminator, while the discriminator is trained to detect generated samples as fake. After the network is fully trained, the losses of both generator and discriminator, defined as:

$$L_{\text{g}} = -\mathbb{E}_{y' \sim P_{\text{G}}} \left[D(y'|x) \right] \tag{2}$$

$$L_{\text{d}} = \mathbb{E}_{y' \sim P_{\text{G}}} \left[D(y'|x) \right] - \mathbb{E}_{y \sim P_{\text{data}}} \left[D(y|x) \right] \tag{3}$$

are minimized and stabilized. Once both generator and discriminator are constructed with enough capacity, the stabilized losses indicate that their performance has plateaued, because P_{G} already equals P_{data}. At this point, the generator can generate samples, y', virtually identical to the real samples, y, (under the conditions x) such that the discriminator is unable to differentiate between them. Detailed flow diagrams of the discriminator and generator are shown in Figure 1b. We used the Leaky ReLu-BatchNorm-transposed convolution modules[55,56] for the generator, and the ReLu-BatchNorm-convolution modules for the discriminator (see Section 1, Supporting Information for detailed network architectures).

Without loss of generality, the all-dielectric meta-atom under consideration is made by patterning a 1-μm-thick film of dielectric material with a refractive index of 5 placed on a dielectric substrate with a refractive index of 1.4. The unit cell size was set to be $2.8 \times 2.8\ \mu m^2$, which is designed to operate in the 5–10 μm spectral range (Figure 1b, left side). Each meta-atom

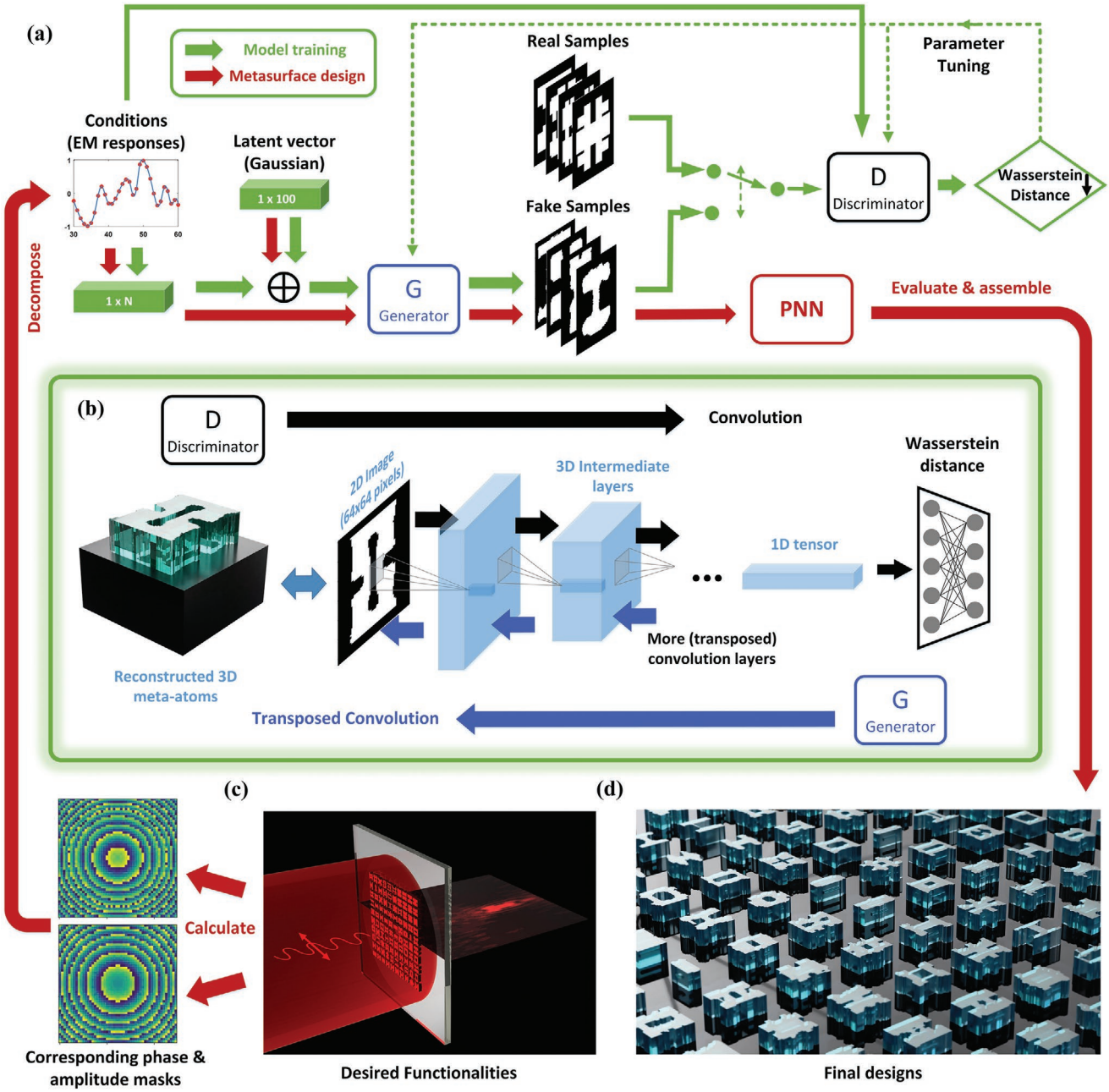

Figure 1. Network architecture of the generative meta-atom design network. a) Schematic diagram of the proposed network. The discriminator network measures the Wasserstein distance between real and fake samples and aims to maximize the distance between them. The generator network attempts to confuse the discriminator by transforming target conditions combined with noise prior to producing fake samples that resemble real ones. Both components approach the ground truth through parameter tuning during this adversarial process. b) Flow diagram of the generator and discriminator: Detailed network structures, including kernel size and output tensor shapes are included in the Section 1, Supporting Information. c) An example of the design process employing the well-trained model. The desired functionalities (lens, deflector, etc.) are translated into phase and amplitude masks, and later fed into the generator to generate actual meta-atom arrays satisfying the design goals. d) Rendered illustration of an exemplary metasurface design assembled with GAN-designed meta-atoms.

was generated with the "needle drop" approach to maximize the accessible pattern diversity (see Section 2, Supporting Information). As part of the preprocessing, 2D cross-sections of all meta-atom from the training dataset were rescaled into 64 × 64 pixel images and binarized (dielectric parts to ones and voids to zeros) prior being fed into the discriminator for evaluation. The 2D dimensions of each image gradually decreased when passed through (2, 2) stride convolutional layers. The output of each layer is batch-normalized and passed through a ReLU activation function before it is sent to the next layer. The generator takes the conditioned prior noise ($z|x$) as an input which is then provided to seven consecutive transposed

convolutional layers. Each layer is followed by a leaky ReLU activation function for conditioned image generation. After the last transposed convolutional layer, a tan*h* activation function generates an image ready for evaluation. Finally, a pre-trained prediction neural network[57] characterizes these output images and eliminates the unqualified meta-atom designs.

Conditions of the proposed generative network structure are formed with single or multiple correlated/uncorrelated EM targets, and therefore this network is uniquely applicable to multifunctional meta-atom/metasurface designs. To explore the potential of our network architecture, we constructed and trained a single wavelength meta-atom design network and a multifunctional metasurface design network, which were used for design and verification of a bifocal lens, a polarization-multiplexed deflector, a polarization-multiplexed lens, and a polarization-independent lens (some of these devices are presented in the Supporting Information).

A meta-atom design network was developed to generate meta-atom patterns based on conditioned phase and amplitude profiles following the proposed network architecture. Due to the phase-related design difficulties as mentioned in ref. [33], a preprocessing layer that translates relative phase and amplitude responses into complex transmission coefficients was added before the first layer of inputs. The real and imaginary parts of the transmission coefficients form the conditions x, such that $x = [T_{\text{real}}(y), T_{\text{imag}}(y)]$. Specifically customized for the meta-atom design task, a novel gradient penalty approach was also adopted to further stabilize the training process (see Section 3, Supporting Information). Without loss of generality, the operating frequency was set to be 50 THz (6 μm wavelength). After 1500 epochs of training, both the discriminator and generator losses were minimized and stabilized (hyperparameters and training curves are included in Section 4, Supporting Information), indicating that the network is fully trained. Unlike traditional GANs, which largely rely on the tuning of the hyperparameters to stabilize the training, the proposed network is highly stable and easily converges. Common training problems with GANs, like gradient explosions and vanishings, were not experienced during the training process regardless of the learning rate, optimizer type, number of layers, etc.

Several randomly selected phase and amplitude combinations were chosen to test the trained network model. For each phase and amplitude combination, we employed the well trained GAN to consecutively generate 100 qualified designs to check the generation stability and efficiency of the proposed approach. **Figure 2** presents several randomly selected phase and amplitude combinations (marked with red dots). The EM responses of the generated patterns were computed using full-wave simulation tools and are labeled with blue dots. We set a minimum threshold of ±0.1 amplitude error and ±10°phase error, as outlined by red lines in each polar plot of Figure 2. The qualified designs for each target are highlighted in yellow, while designs with performance that fall outside the red outlines are left dark. As shown in Figure 2, given the specific amplitude and phase targets, numerous qualified meta-atom designs of various shapes can be generated within a few seconds, manifesting the proposed design approach is highly time efficient. Having only one unqualified design among 600 extracted meta-atoms (Figure 2c) indicates the network's high generalization stability and accuracy.

The ability to design on demand meta-atom geometries with the specified phase and amplitude responses enables various striking applications, including multi-focal metalenses,[10] beam deflectors,[58] holograms,[3,59] and airy beam generators.[10,12] Using the trained network, we designed a bifocal metalens operating at 50 THz, which requires simultaneous amplitude and phase modulations of each meta-atom within the metalens. To reduce the complexity of full-wave based verification process, the size of this metalens is limited to 50 × 50 meta-atoms (140 μm by 140 μm). For the designed bifocal lens with two focal points (f_1 and f_2) aligned laterally, the phase and amplitude profiles at (x_0,y_0) on the metalens are given by:

$$\mathrm{a}\left(x_0, y_0\right) e^{j\varphi(x_0,y_0)} = \frac{a_1}{d_1}\exp^{j\frac{2\pi}{\lambda}d_1} + \frac{a_2}{d_2}\exp^{j\frac{2\pi}{\lambda}d_2} \tag{4}$$

where d_1 and d_2 are the distance between the point (x_0,y_0) and two focal points f_1 and f_2, respectively, a_1 and a_2 are the amplitudes for the two focal points. In this demonstration, we set $f_1 = f_2 = 60$ μm and $a_1 = a_2 = 1$. Two focal points are separated by a lateral distance (along the x-axis) $d = 60$ μm. The calculated amplitude and phase masks are plotted in **Figure 3**a,b, respectively, illustrating the requirements for independent amplitude and phase control. In order to demonstrate the ideal (theoretical) performance of this dual focal lens, we theoretically calculated and plotted the electric field distribution in the x–z plane at $y = 0$ (Figure 3c) by modeling each meta-atom as a linearly polarized point source with the amplitude and phase values taken from Figure 3a,b. The two E_x field maxima occur as expected by the design at the two focal spots that are 60 μm away from the metasurface plane.

The amplitude and phase design targets for each meta-atom are designated as inputs to the GAN, while the output qualified meta-atom designs are used to assemble the whole device. The final metasurface design, along with the amplitude and phase profiles for each meta-atom as verified by numerical simulations, is shown in Figure 3d,e, respectively. The electric field distribution produced by this metalens was also modeled using full-wave simulations (Figure 3f). This design demonstration highlights the three key advantages of our approach: 1) Over 600 qualified free-form meta-atoms were generated in less than 1 min, indicating its time efficiency; 2) the excellent agreement between targeted (Figure 3a,b) and simulated (Figure 3e) meta-atom performances, as well as the agreement between the theoretical calculation (Figure 3c) and the full-wave simulation result (Figure 3f), validates its accuracy; and 3) considering almost all target functionalities can be decomposed into specific phase and amplitude requirements on the meta-atom level, this design approach can be easily extended for the design of various other devices including beam deflectors and holograms demonstrating that it is scalable and universal.

Due to the network condition vector's high flexibility, the network structure can be easily adapted to generate meta-atom geometries for implementing multifunctional metasurfaces. For example, by enlarging and rearranging the condition vector: $x = [T_{\text{real}}(y_{\text{p1}}), T_{\text{imag}}(y_{\text{p1}}), T_{\text{real}}(y_{\text{p2}}), T_{\text{imag}}(y_{\text{p2}})]$, the network can be configured as a dual-polarization meta-atom design network. Moreover, after being fully trained on the data of complex transmission coefficients associated with two orthogonal linear

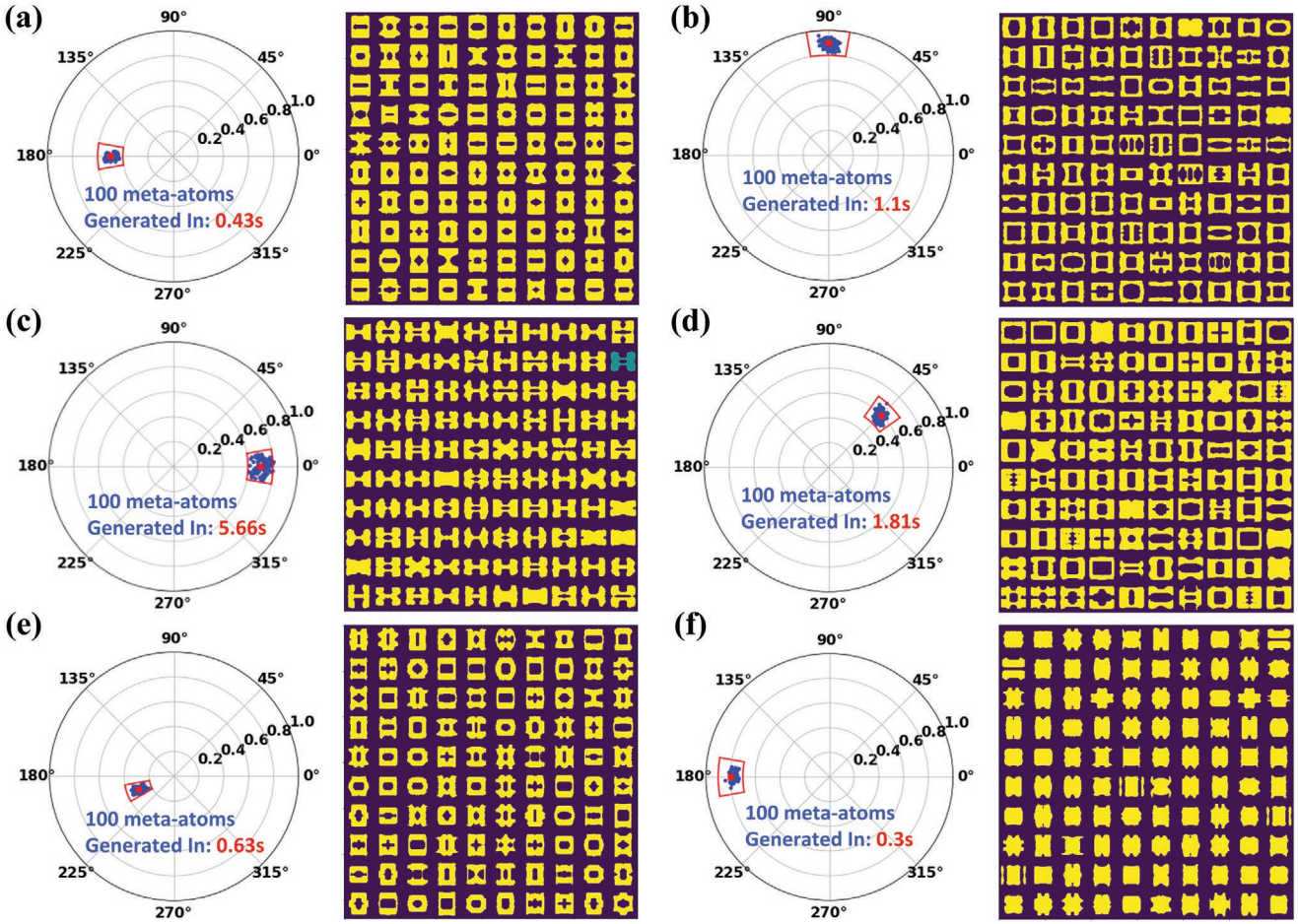

Figure 2. Meta-atom designs generated using a fully-trained conditional WGAN model. 100 meta-atom designs were produced for each combined condition of amplitude and phase: a) 0.5 + 180°, b) 0.9 + 90°, c) 0.7 + 0°, d) 0.6 + 45°, e) 0.3 + 200°, and f) 0.8 + 180°, respectively. In the polar charts the radial and angular coordinates correspond to the transmission amplitude and phase. Blue dots represent EM responses of generated designs, red dots represent the targeted amplitude and phase conditions. 2D patterns of meta-atoms from each design group are shown on the right side of each subplot. Red outlines indicate the bounds of the allowed phase-amplitude values, while the corresponding qualified patterns are highlighted in yellow. Illumination of each meta-atom is performed from with an *x*-polarized plane wave from the substrate side.

polarizations (along *x* and *y* axes) (e.g., at 55 THz), the proposed generative network is able to compose meta-atom designs based on four distinct inputs: Amplitude and phase responses for incident waves with two orthogonal polarization directions (in this case *x*-polarized and *y*-polarized). Notably, with a condition vector containing four different design targets, it's nearly impossible to achieve a high-performance design by using the traditional empirical trial-and-error design approaches, since a slight change in the shape of the meta-atom will affect the four design outcomes simultaneously. With the proposed deep learning approach, we were able to find qualified designs in seconds. Similarly, as for the meta-atom design network, a comprehensive set of phase and amplitude targets for two orthogonal polarizations were chosen to test the performance of the trained network model.

As an example, we set the design goal for a horizontal polarization to a specific amplitude-phase value (0.9, 0°) and gradually varied the targeted phase for the orthogonal polarization from 45° to 315° (with a 90° step). For each amplitude-phase value, we employed the combined network to consecutively generate 100 qualified meta-atom geometries to verify its generation stability and time efficiency for this type of task. The EM responses of generated meta-atoms were simulated and labeled with red and blue dots in **Figure 4**a–d. We adopted a minimum threshold of ± 0.1 and ± 10° for amplitude and phase errors. The allowed values are outlined in red and blue lines in each polar plot of Figure 4a–d. Evidently, the stricter design targets have limited the design DOF and reduced the design space, which led to increased similarities between qualified meta-atom shapes in Figure 4b,c. This also increased the difficulty of finding a qualified design, which manifested in a relatively longer pattern generation time (e.g., 32 s in Figure 4a for generating 100 qualified designs) compared to the single-target meta-atom designs shown in Figure 2.

After the proposed multifunctional meta-atom design network has been fully trained, we demonstrated its performance through generating several multifunctional meta-device designs working in the mid-IR range. Figure 4e–f displays the top-view and 3D-view of a polarization-multiplexed beam deflector. The designed beam deflector consists of four meta-atom designs

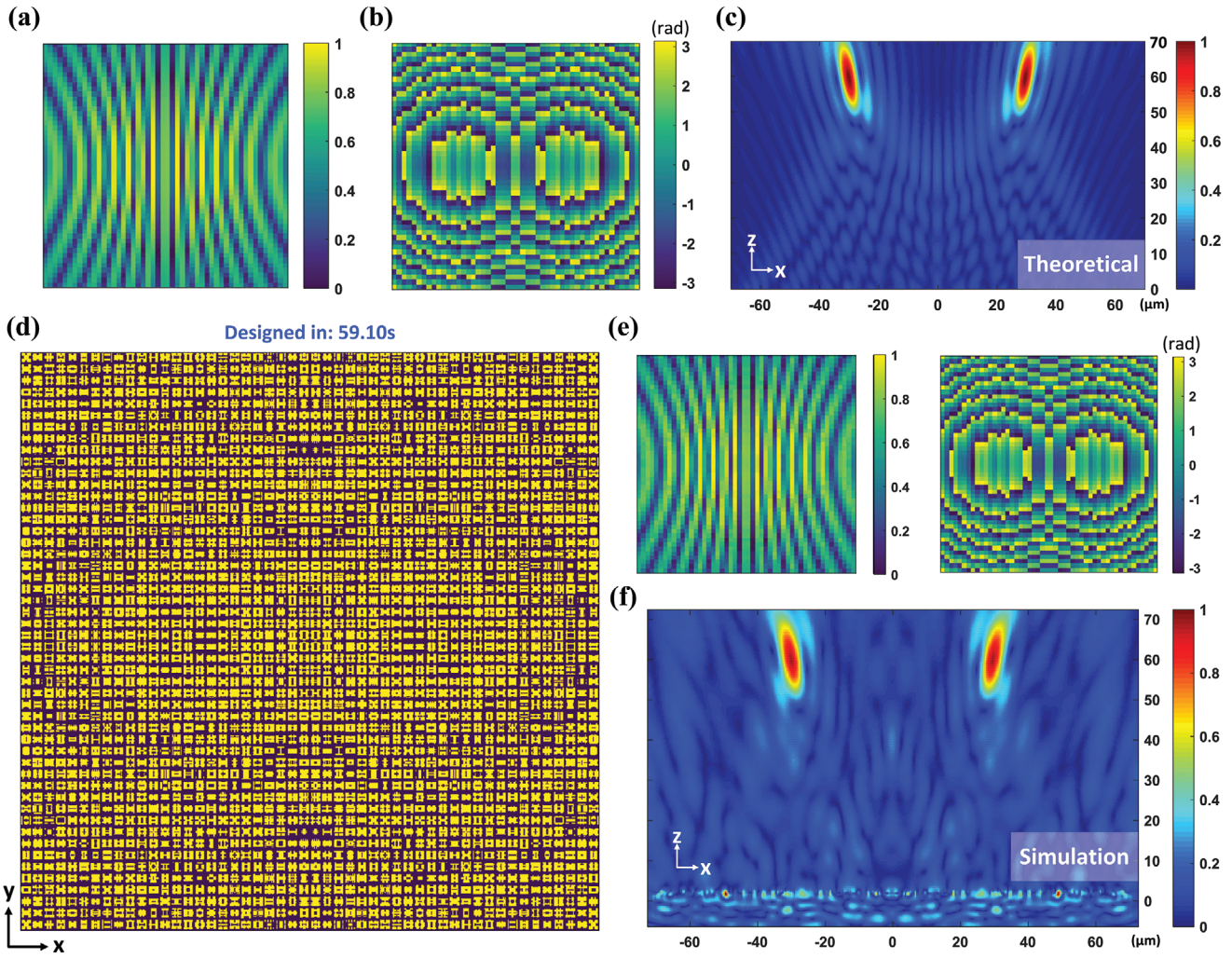

Figure 3. A bifocal lens designed with the meta-atom generative network. a) Target amplitude mask and b) target phase mask of the designed lateral bifocal metalens at 50 THz with $f_1 = f_2 = 60$ μm. c) Theoretical E_x field distributions in the *x*–*z* plane calculated with MATLAB. d) Metasurface pattern designed by the meta-atom generative network. Since the target *E*-field is symmetrical along *x* and *y* axes, only one quadrant of the metasurface lens was designed, with the rest being generated from symmetry by mirroring along the *x* and *y* axes. e) Amplitude and phase masks for corresponding meta-atoms in (d). f) Full-wave simulation results of the E_x field in the *x*–*z* plane.

selected from each set of 100 geometries in Figure 4a–d. The four meta-atoms form a supercell and are tiled along both the *x* and *y* directions with periods of 11.2 and 2.8 μm, respectively. When illuminated with *y*-polarized plane waves (Figure 4g), all meta-atoms have the same phase delays and hence no diffraction beyond the 0th order (specular transmission) appears. With *x*-polarized plane wave incidence (Figure 4h), the whole structure acts as a diffractive grating along the *x*-axis due to the 90-degree-step phase gradient (resembling a traditional blazed grating) to selectively enhance the first diffraction order while suppressing all others. Simulated E-field radiation patterns and E-field amplitude profiles under incidences with different polarization directions are plotted in Figure 4g,h. It is clearly shown that under *x*-polarized incidence light, most of the optical power is concentrated in the first transmissive diffraction order (at the theoretical deflection angle of 29.14 degrees).

Lastly, a polarization-multiplexed bifocal metalens was designed using the proposed multifunctional meta-atom design network (**Figure 5**). The metalens was designed with a focal length of 60 μm under *y*-polarized plane wave incidence (Figure 5a) and 80 μm focal length when illuminated with an *x*-polarized plane wave (Figure 5b). The target phase maps of the lens under both *x*- and *y*-polarized incidence were calculated separately and used as phase inputs for the generative network (first row in Figure 5d), while the amplitude profiles are kept uniform to maximize the focusing efficiency. Actual phase responses under *x*- and *y*-polarized incidences for each meta-atom are simulated and also presented in Figure 5d (second row) for comparison. The electric fields in the *y*–*z* plane corresponding to the two different polarization directions were computed by full wave simulation and are plotted in Figure 5e, where a clear focal spot at the desired focal length is observed for each case. The electric fields along the optical axis were also simulated and plotted in Figure 5f, where two distinct electric field peaks can be clearly observed at 60 and 80 μm, respectively. Similarly, we can also easily design a polarization-independent

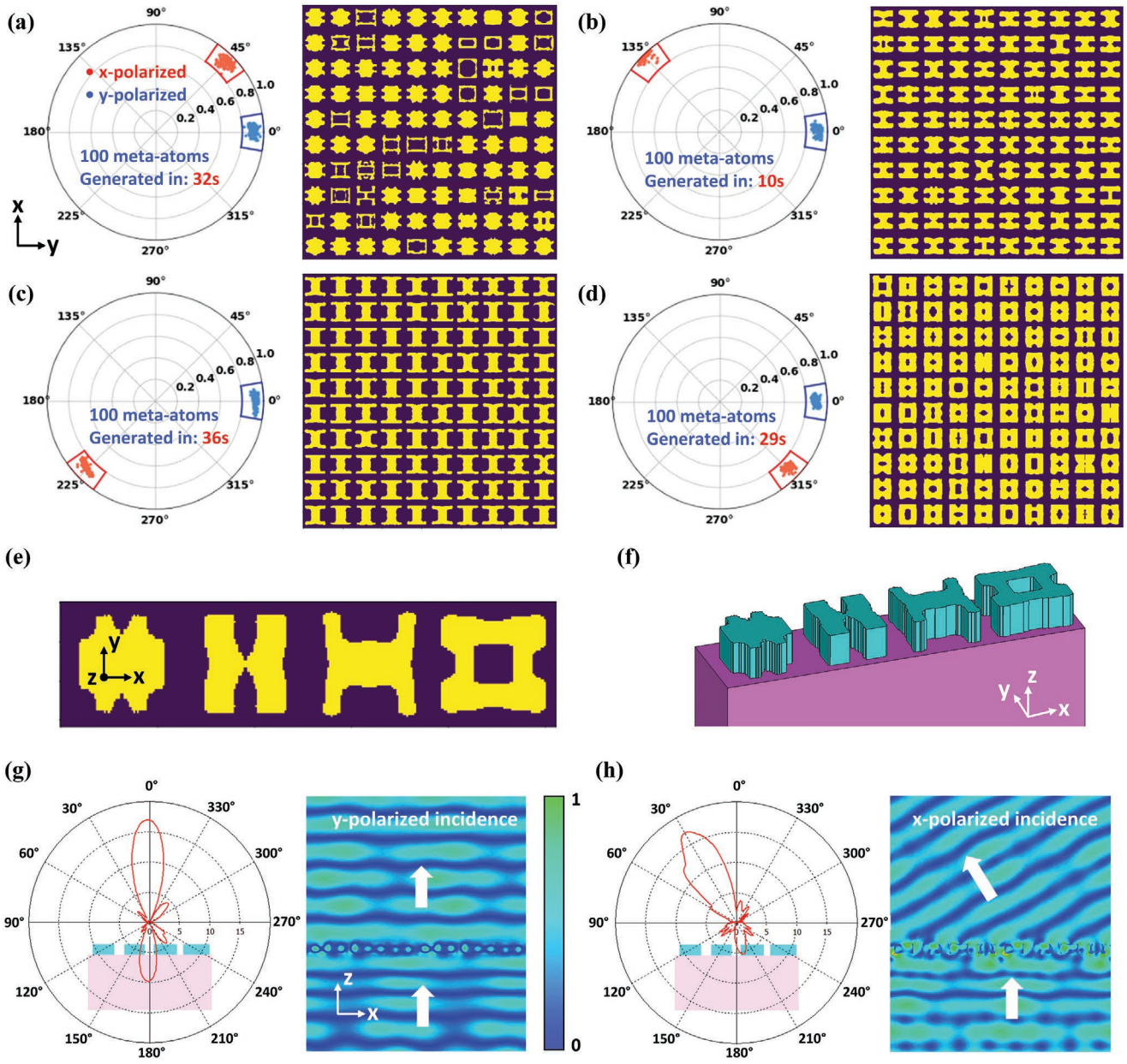

Figure 4. Multifunctional meta-atom designs generated using a fully-trained GAN model. EM responses of the generated 100 meta-atoms for two orthogonal polarizations: a) *y*-polarization (blue dots): 0.9 + 0°, *x*-polarization (red dots): 0.9 + 45°; b) *y*-polarization: 0.9 + 0°, *x*-polarization: 0.9 + 135°, c) *y*-polarization: 0.9 + 0°, *x*-polarization: 0.9 + 225°, and d) *y*-polarization: 0.9 + 0°, *x*-polarization: 0.9 + 315°. Red and blue outlines in each polar plot indicate qualified responses under different polarizations, with corresponding patterns highlighted in yellow. e) Top view and f) 3D view of a polarization-multiplexed beam deflector assembled with the designed meta-atoms. g) Simulated E-field angular radiation pattern and E_y field results for a *y*-polarized plane wave incidence. h) Simulated E-field angular radiation pattern and E_x field results for an *x*-polarized plane wave incidence.

lens utilizing the same generative network (Section 5, Supporting Information).

The ability of the proposed network to precisely achieve the multifunctional design goals, as shown in Figures 2 and 4, along with the performances of the assembled metasurface devices shown in Figures 3–5, have verified the utility, power, and ease of use for this approach. The presented approach is much more effective compared to trial-and-error and exhaustive search methods, meanwhile provides a promising alternative solution for conventional optimization design approaches since: 1) Once the training is completed, the GAN approach is able to generate on-demand designs with almost zero time cost, and no additional full-wave simulations are needed during the design process. 2) Our GAN generates designs with stable performances and does not depend on the initial guess of the meta-atoms' shapes and other parameters. Moreover, meta-atom designs derived with the proposed approach can be specified as high-quality initial designs and further refined with optimization algorithms, which provides a potential solution for addressing the local minima optimization

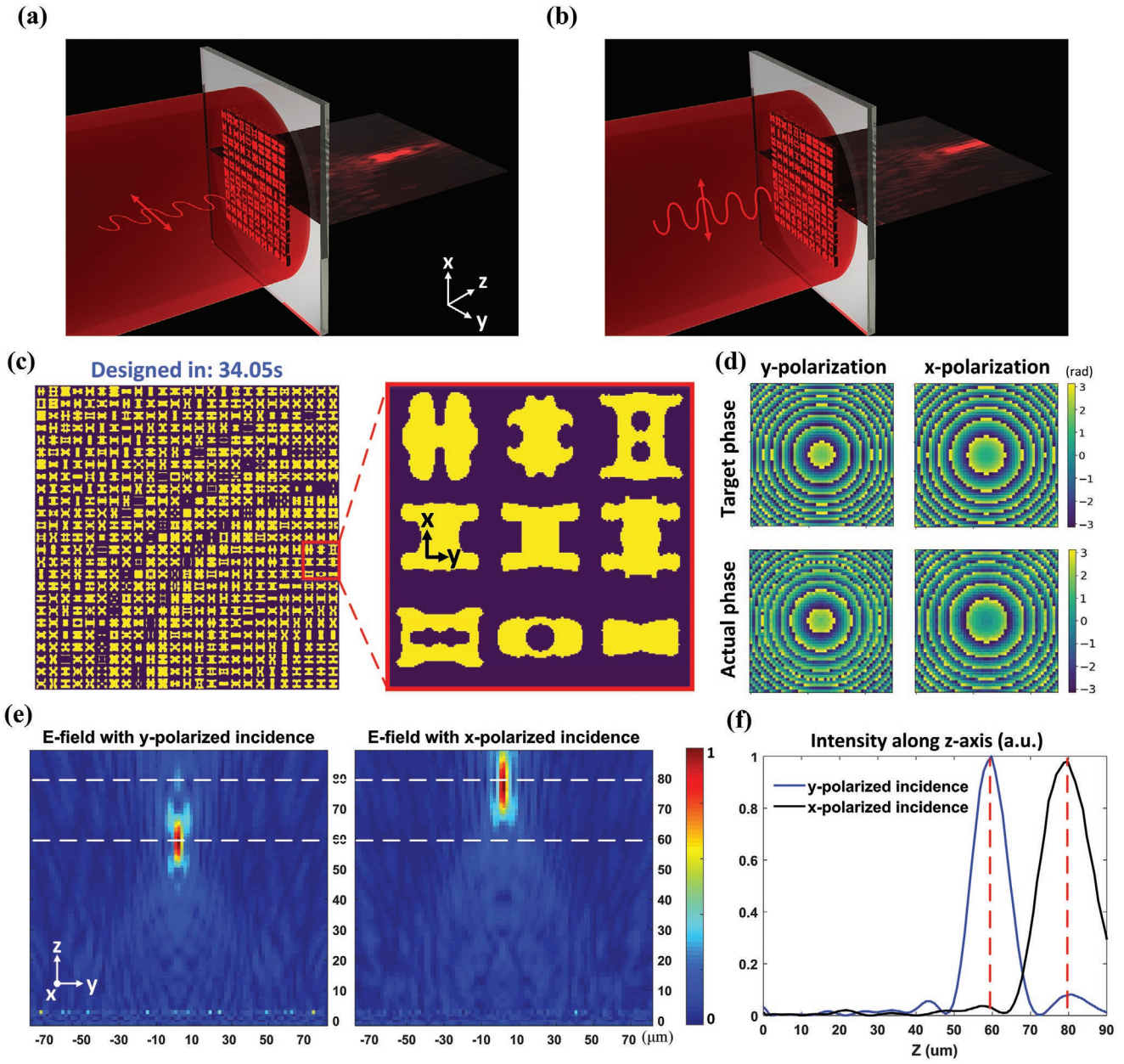

Figure 5. A polarization-multiplexed metalens designed with the dual-polarization meta-atom generative network. The lens has a 140 μm × 140 μm aperture size, containing 50 × 50 meta-atoms in total. 3D illustration demonstrating the metalens functionality under a) *y*- and b) *x*-polarized incident light. c) Metasurface pattern designed with the dual-polarization meta-atom generative network. Only the top left quadrant of the lens was generated, with the rest being duplicated according to the design symmetry. d) Target (first row) and actual simulated (second row) phase masks for the bifocal lens for each polarization incidence. e) Full-wave simulated E-field in *y*–*z* plane under *y* and *x*-polarized incidence, respectively. The focal spot is shifted from $z = 60$ to 80 μm when the polarization direction switched from *y* to *x*. f) Simulated E-field intensity along the optical axis.

problems. 3) By training the proposed GAN with data collected from meta-atoms with various refractive indexes, thicknesses, lattice sizes, 2D cross sections, and loss factors, the proposed approach can be easily extended to a variety of metasurface platforms based on different materials and fabrication processes. 4) The condition vector in the proposed GANs are highly versatile and can be easily customized into various multifunctional design goals, which remains a major challenge to traditional design approaches. Aside from the polarization-multiplexed metasurface designs presented in the paper, the proposed network structure can also be easily customized for designing other multifunctional devices including multi-band meta-atom/metasurfaces, wideband meta-filters, tunable meta-devices, and many more (Section 6, Supporting Information). Moreover, due to the generative nature of the proposed network, the well-trained model can create massive numbers of meta-atom designs (for the same design target) in a short time period (e.g., a few milliseconds or less). This feature allows us to select

robust meta-atoms which are insensitive to the fabrication defects such as refractive index variations, surface roughness, and non-vertical sidewalls. An example about how different meta-atoms with identical performance can suffer differently from non-vertical sidewall angles is shown in Section 7, Supporting Information.

In addition to its use for meta-device design, the proposed GAN may be a useful tool for topological analysis of meta-atom structures. Examination of classes of structures generated by the proposed network that share a particular EM response (as shown in Figure 2)[60,61] can lead to the discovery of underlying physical characteristics. By processing the image through several convolutional layers, the neural network can uncover the common traits of these designs; these common traits can be used to categorize the designs into the same conditional distribution, which is highly non-intuitive. Designs with inclined edges and round corners are generated (Figure 2a–f), despite that training datasets collected with the "needle drop" approach are all composed of rectangles with straight sharp edges and limited to only 28×28 resolution. This result highlights the exploratory (learning and composing) nature of the proposed network, which utilizes the increased 64×64 image resolution to yield design details that are not included in the training data and transcend training data limitations.

To conclude, we have proposed a metasurface design network based on the conditional WGAN architecture that is capable of efficiently producing numerous multifunctional meta-device designs on demand. The fully-trained network demonstrated this capability through several example designs, including a bifocal metalens, a polarization-multiplexed beam deflector, a polarization-multiplexed metalens, and a polarization-independent metalens. Excellent agreement has been achieved between design targets and generated device performance for each design. Furthermore, we suggest that the proposed network can be used as a tool for topological analysis in uncovering shared physical features within groups of similar EM responses. We envision that this deep-learning-based design approach can be readily applied beyond multifunctional metasurfaces/meta-atoms to various types of other multifunctional EM devices, such as microwave components, antennas, and integrated optical circuits.

Supporting Information

Supporting Information is available from the Wiley Online Library or from the author.

Acknowledgements

This work was funded under Defense Advanced Research Projects Agency Defense Sciences Office (DSO) Program: EXTREME Optics and Imaging (EXTREME) under Agreement No. HR00111720029.

Conflict of Interest

The authors declare no conflict of interest.

Data Availability Statement

Research data are not shared.

Keywords

deep learning, inverse design, metasurfaces, neural networks, photonics

Received: August 20, 2020
Revised: December 23, 2020
Published online: January 20, 2021

[1] H. C. van de Hulst, *Light Scattering by Small Particles*, Courier Corporation, North Chelmsford, USA **1981**.
[2] J. D. Jackson, *Classical Electrodynamics*, 3rd ed., John Wiley & Sons, Hoboken, USA **2007**.
[3] Q. Wang, X. Zhang, Y. Xu, J. Gu, Y. Li, Z. Tian, R. Singh, S. Zhang, J. Han, W. Zhang, *Sci. Rep.* **2016**, *6*, 32867.
[4] A. Arbabi, Y. Horie, M. Bagheri, A. Faraon, *Nat. Nanotechnol.* **2015**, *10*, 937.
[5] N. Yu, F. Capasso, *Nat. Mater.* **2014**, *13*, 139.
[6] L. Zhang, J. Ding, H. Zheng, S. An, H. Lin, B. Zheng, Q. Du, G. Yin, J. Michon, Y. Zhang, Z. Fang, M. Y. Shalaginov, L. Deng, T. Gu, H. Zhang, J. Hu, *Nat. Commun.* **2018**, *9*, 1481.
[7] S. Jahani, Z. Jacob, *Nat. Nanotechnol.* **2016**, *11*, 23.
[8] M. Khorasaninejad, Z. Shi, A. Y. Zhu, W.-T. Chen, V. Sanjeev, A. Zaidi, F. Capasso, *Nano Lett.* **2017**, *17*, 1819.
[9] X. Wang, J. Ding, B. Zheng, S. An, G. Zhai, H. Zhang, *Sci. Rep.* **2018**, *8*, 1876.
[10] J. Ding, S. An, B. Zheng, H. Zhang, *Adv. Opt. Mater.* **2017**, *5*, 1700079.
[11] T. Wang, R. Xie, S. Zhu, J. Gao, M. Xin, S. An, B. Zheng, H. Li, Y. Lin, H. Zhang, G. Zhai, J. Ding, *IEEE Access* **2019**, *7*, 58131.
[12] L. Liu, X. Zhang, M. Kenney, X. Su, N. Xu, C. Ouyang, Y. Shi, J. Han, W. Zhang, S. Zhang, *Adv. Mater.* **2014**, *26*, 5031.
[13] D. Sell, J. Yang, S. Doshay, J. A. Fan, *Adv. Opt. Mater.* **2017**, *5*, 1700645.
[14] H. Cheng, X. Wei, P. Yu, Z. Li, Z. Liu, J. Li, S. Chen, J. Tian, *Appl. Phys. Lett.* **2017**, *110*, 171903.
[15] F. Callewaert, V. Velev, P. Kumar, A. Sahakian, K. Aydin, *Sci. Rep.* **2018**, *8*, 1358.
[16] C. H. Chu, M. L. Tseng, J. Chen, P. C. Wu, Y. H. Chen, H. C. Wang, T. Y. Chen, W. T. Hsieh, H. J. Wu, G. Sun, D. P. Tsai, *Laser Photonics Rev.* **2016**, *10*, 986.
[17] M. Y. Shalaginov, S. An, Y. Zhang, F. Yang, P. Su, V. Liberman, J. B. Chou, C. M. Roberts, M. Kang, C. Rios, Q. Du, C. Fowler, A. Agarwal, K. Richardson, C. Rivero-Baleine, H. Zhang, J. Hu, T. Gu, arXiv:1911.12970, **2019**.
[18] Y. Zhang, J. B. Chou, J. Li, H. Li, Q. Du, A. Yadav, S. Zhou, M. Y. Shalaginov, Z. Fang, H. Zhong, C. Roberts, P. Robinson, B. Bohlin, C. Rios, H. Lin, M. Kang, T. Gu, J. Warner, V. Liberman, K. Richardson, J. Hu, *Nat. Commun.* **2019**, *10*, 4279.
[19] M. Y. Shalaginov, S. D. Campbell, S. An, Y. Zhang, C. Ríos, E. B. Whiting, Y. Wu, L. Kang, B. Zheng, C. Fowler, H. Zhang, D. H. Werner, J. Hu, T. Gu, *Nanophotonics* **2020**, *9*, 3505.
[20] Y. Zhang, C. Fowler, J. Liang, B. Azhar, M. Y. Shalaginov, S. An, J. B. Chou, C. M. Roberts, V. Liberman, M. Kang, C. Rios, K. A. Richardson, C. Rivero-Baleine, T. Gu, H. Zhang, J. Hu, arXiv:2008.06659, **2020**.
[21] Y. Zhang, J. Liang, M. Shalaginov, S. Deckoff-Jones, C. Ríos, J. B. Chou, C. Roberts, S. An, C. Fowler, S. D. Campbell, B. Azhar, C. Goncalves, K. A. Richardson, H. Zhang, D. H. Werner, T. Gu, J. Hu, presented at *CLEO: Science and Innovations*, San Jose,USA, May **2019**.

[22] R. C. Devlin, M. Khorasaninejad, W. T. Chen, J. Oh, F. Capasso, *Proc. Natl. Acad. Sci. USA* **2016**, *113*, 10473.
[23] E. Arbabi, A. Arbabi, S. M. Kamali, Y. Horie, A. Faraon, *Optica* **2016**, *3*, 628.
[24] D. Z. Zhu, E. B. Whiting, S. D. Campbell, D. B. Burckel, D. H. Werner, *ACS Photonics* **2019**, *6*, 2741.
[25] S. D. Campbell, E. B. Whiting, D. H. Werner, P. L. Werner, presented at *2019 Int. Applied Computational Electromagnetics Society Symp. (ACES)*, Miami, USA, May **2019**.
[26] Z. Liu, D. Zhu, K. T. Lee, A. S. Kim, L. Raju, W. Cai, *Adv. Mater.* **2020**, *32*, 1904790.
[27] E. B. Whiting, S. D. Campbell, L. Kang, D. H. Werner, *Opt. Express* **2020**, *28*, 24229.
[28] D. Liu, Y. Tan, E. Khoram, Z. Yu, *ACS Photonics* **2018**, *5*, 1365.
[29] Z. Liu, D. Zhu, S. P. Rodrigues, K.-T. Lee, W. Cai, *Nano Lett.* **2018**, *18*, 6570.
[30] W. Ma, F. Cheng, Y. Liu, *ACS Nano* **2018**, *12*, 6326.
[31] I. Malkiel, M. Mrejen, A. Nagler, U. Arieli, L. Wolf, H. Suchowski, *Light: Sci. Appl.* **2018**, *7*, 60.
[32] J. Peurifoy, Y. Shen, L. Jing, Y. Yang, F. Cano-Renteria, B. G. DeLacy, J. D. Joannopoulos, M. Tegmark, M. Soljačić, *Sci. Adv.* **2018**, *4*, eaar4206.
[33] S. An, C. Fowler, B. Zheng, M. Y. Shalaginov, H. Tang, H. Li, L. Zhou, J. Ding, A. M. Agarwal, C. Rivero-Baleine, K. A. Richardson, T. Gu, J. Hu, H. Zhang, *ACS Photonics* **2019**, *6*, 3196.
[34] S. So, J. Mun, J. Rho, *ACS Appl. Mater. Interfaces* **2019**, *11*, 24264.
[35] R. S. Hegde, in *Proc. SPIE 11105, Novel Optical Systems, Methods, and Applications XXII*, SPIE, Bellingham, USA **2019**, p. 1110508.
[36] Z. Liu, Z. Zhu, W. Cai, *Opt. Express* **2020**, *28*, 4825.
[37] J. Hao, L. Zheng, D. Yang, Y. Guo, presented at *Asia Communications and Photonics Conference*, Chengdu, China, November **2019**.
[38] K.-F. Lin, C.-C. Hsieh, S.-C. Hsin, W.-F. Hsieh, *Appl. Opt.* **2019**, *58*, 8914.
[39] X. Han, Z. Fan, C. Li, Z. Liu, L. J. Guo, arXiv:1912.03696, **2019**.
[40] I. Goodfellow, J. Pouget-Abadie, M. Mirza, B. Xu, D. Warde-Farley, S. Ozair, A. Courville, Y. Bengio, in *NIPS'14: Proceedings of the 27th Int. Conf. on Neural Information Processing Systems*, MIT Press, Cambridge, **2014**, pp. 2672–2680.
[41] M. Mirza, S. Osindero, arXiv:1411.1784, **2014**.
[42] W. Ma, Y. Liu, *Sci. China: Phys., Mech. Astron.* **2020**, *63*, 237011.
[43] S. So, J. Rho, *Nanophotonics* **2019**, *8*, 1255.
[44] Z. A. Kudyshev, A. V. Kildishev, V. M. Shalaev, A. Boltasseva, *Appl. Phys. Rev.* **2020**, *7*, 021407.
[45] J. Jiang, J. A. Fan, arXiv:1906.07843, **2019**.
[46] J. Jiang, J. A. Fan, *Nano Lett.* **2019**, *19*, 5366.
[47] J. Jiang, D. Sell, S. Hoyer, J. Hickey, J. Yang, J. A. Fan, *ACS Nano* **2019**, *13*, 8872.
[48] W. Ma, F. Cheng, Y. Xu, Q. Wen, Y. Liu, *Adv. Mater.* **2019**, *31*, 1901111.
[49] S. So, J. Rho, *Nanophotonics* **2019**, *8*, 1255.
[50] J. A. Hodge, K. V. Mishra, A. I. Zaghloul, presented at *2019 IEEE 29th Int. Workshop on Machine Learning for Signal Processing (MLSP)*, IEEE, Piscataway, NJ **2019**, pp. 1–6.
[51] J. A. Hodge, K. V. Mishra, A. I. Zaghloul, presented at *2019 IEEE Global Conf. on Signal and Information Processing*, IEEE, Piscataway, NJ **2019**, pp. 1–5.
[52] I. Sajedian, J. Kim, J. Rho, *Microsyst. Nanoeng.* **2019**, *5*, 27.
[53] M. Arjovsky, S. Chintala, L. Bottou, *Proceedings of the 34th Int. Conf. on Machine Learning*, PMLR, Vol. *70*, International Convention Centre, Sydney, Australia **2017**, pp. 214–223.
[54] I. Gulrajani, F. Ahmed, M. Arjovsky, V. Dumoulin, A. C. Courville, presented at *Advances in Neural Information Processing Systems*, Long Beach, USA, December **2017**.
[55] K. He, X. Zhang, S. Ren, J. Sun, *Proc. of the IEEE Int. Conf. on Computer Vision (ICCV 2015)*, IEEE, Piscataway, NJ **2015**.
[56] S. Ioffe, C. Szegedy, arXiv:1502.03167, **2015**.
[57] S. An, B. Zheng, M. Y. Shalaginov, H. Tang, H. Li, L. Zhou, J. Ding, A. M. Agarwal, C. Rivero-Baleine, M. Kang, K. A. Richardson, T. Gu, J. Hu, C. Fowler, H. Zhang, *Opt. Express* **2020**, *28*, 31932.
[58] J. Ding, N. Xu, H. Ren, Y. Lin, W. Zhang, H. Zhang, *Sci. Rep.* **2016**, *6*, 34020.
[59] H. Ren, W. Shao, Y. Li, F. Salim, M. Gu, *Sci. Adv.* **2020**, *6*, eaaz4261.
[60] Y. Kiarashinejad, S. Abdollahramezani, M. Zandehshahvar, O. Hemmatyar, A. Adibi, arXiv:1905.06889, **2019**.
[61] Y. Kiarashinejad, M. Zandehshahvar, S. Abdollahramezani, O. Hemmatyar, R. Pourabolghasem, A. Adibi, arXiv:1909.07330, **2019**.